Ionics (2021) 27:507–515
https://doi.org/10.1007/s11581-020-03878-x

ORIGINAL PAPER

Nitrogen-doped carbon-coated $Li_3V_2(PO_4)_3$ as cathode materials for high-performance lithium storage

Dexing Zhao[1,2] · Lulu Mo[1,2] · Qing Han[1,2] · Lingling Xie[2,3] · Limin Zhu[1,2] · Xiaoyu Cao[1,2]

Received: 16 November 2020 / Revised: 9 December 2020 / Accepted: 10 December 2020 / Published online: 6 January 2021

Abstract

A series of novel N-doped carbon-coated $Li_3V_2(PO_4)_3$ (LVPC/N) composites were synthesized by rheological phase method with melamine as nitrogen source. The results showed that N-doping did not affect the main structure of $Li_3V_2(PO_4)_3$/C (LVPC) but only changed the structure and properties of the coating layer, which effectively improved the structural stability and electrochemical performance of LVPC. When the ratio of citric acid to melamine was 5:3, the properties of LVPCN composite were the best. The initial discharge specific capacity was 195 mAh g^{-1} at 30 mA g^{-1} in the voltage range of 3.0–4.8 V. After 100 cycles of charge and discharge, the discharge capacity was still 165 mAh g^{-1}, and the capacity retention rate was increased to 85%. Owing to the low cost, high initial discharge capacity, and long lifespan, we believe that the LVPC/N composite is significantly competitive to other cathode materials for application in lithium-ion batteries.

Keywords LVPC/N composites · Low cost · Cathode material · Lithium-ion battery · High performance

Introduction

The development of advanced secondary battery with high specific energy density is an urgent demand in the application fields of portable electronic products, electric vehicles, and large-scale energy storage. Lithium-ion batteries (LIBs) own the most probable prospect as the alternate candidate in the above-mentioned areas because of their high energy, the high power density, and the superior cycling stability [1–6]. Currently, the actual specific capacity of graphite anode material used in commercial LIBs is close to its theoretical value of 372 mAh g^{-1} [7–9], and the specific capacity of the next generation of alloy materials may even exceed 1000 mAh g^{-1}, such as Si-based anode materials [10, 11] and various materials using metal-organic frameworks (MOF) as precursors [12–16]. However, the corresponding commercial cathode materials have low specific capacity, such as $LiCoO_2$ (140–150 mAh g^{-1}) [17–19], $LiFePO_4$ (150–160 mAh g^{-1}) [20–22], and $LiMn_2O_4$ (110–130 mAh g^{-1}) [23–25]. So, we can see that LIBs suffer from the low specific capacities of cathode materials. Therefore, the development of high capacity cathode materials has become the key technology for upgrading the LIBs.

Monoclinic $Li_3V_2(PO_4)_3$ (LVP) has attracted much attention due to its high theoretical capacity (a theoretical capacity of 132 mAh g^{-1} can be obtained in the range of 3.0–4.3 V, and the theoretical capacity can be as high as 197 mAh g^{-1} in the range of 3.0–4.8 V), low synthesis cost, stable structure, and simple synthesis method [26, 27]. However, the main problem of this material is its low electronic conductivity, which is only about 2.4×10^{-7} S cm^{-1} at room temperature. Previous studies have shown that carbon coating or compositing can overcome the above disadvantages of LVP [28–31]. However, this is still unable to meet the demand in the field of high voltage, high power, and long working time power battery, which urges researchers to seek more effective methods to further improve the high rate performance and cycle life of LVP.

Dexing Zhao and Lulu Mo contributed equally to this work.

✉ Limin Zhu
lmzhu@haut.edu.cn

✉ Xiaoyu Cao
caoxy@haut.edu.cn

[1] School of Chemistry and Chemical Engineering, Henan University of Technology, Zhengzhou 450001, People's Republic of China

[2] Key Laboratory of High Specific Energy Materials for Electrochemical Power Sources of Zhengzhou City, Henan University of Technology, Zhengzhou 450001, People's Republic of China

[3] School of Environmental Engineering, Henan University of Technology, Zhengzhou 450001, People's Republic of China

In recent years, the use of N-doped carbon materials to modify lithium-ion electrode materials has attracted extensive attention. This kind of carbon materials are mainly focused on graphite, graphene, and carbon nanotubes [32–36]. The principle of nitrogen-doped carbon coating modification is mainly reflected in the following aspects: (1) N-doping can modify the structure, chemical activity, and electronic properties of the materials; (2) N-doping can produce many extrinsic defects and active sites; and (3) nitrogen/carbon co modification can improve the stability of SEI film [37–39]. As far as we know, there are also reports that N-doped carbon materials, such as N-doped graphite and graphene, are used to modify LVP to improve its electrochemical performance. However, these N-doped carbon materials need complex nitrogen doping modification process, and the efficiency is also low. Based on this, in this work, we designed a simple rheological phase method, using melamine as nitrogen source and citric acid as carbon source to synthesize nitrogen carbon co coated LVP composites, and studied the effect of N-doping on the phase structure, morphology, and electrochemical properties of $Li_3V_2(PO_4)_3$/C (LVPC).

Experimental

$LiOH{\cdot}H_2O$, V_2O_5, $NH_4H_2PO_4$, citric acid, and melamine with a stoichiometric ratio of 3.1:1:3:2-*x*:*x* (*x* = 0, 0.25, 0.5, 0.75, and 1) (by molar) were accurately weighed as lithium, vanadium, phosphorus, carbon, and nitrogen sources. Put the above raw materials in a dry agate mortar, fully grind the raw materials to fine powder under an infrared lamp, and mix them evenly. Then the raw materials were transferred to the PVC lining, and deionized water was added dropwise in the lining to adjust the powder raw materials to the rheological phase state. Then the lining was put into the reactor, tightly sealed, and put into the oven at 80 °C for 6 h. After that, the reactor was taken out for natural cooling and obtained bright blue-green viscous slurry and then dried in a drying oven at 100 °C for 12 h, and the blue-green honeycomb N-doped LVPC precursor was obtained. The dried precursor was taken out and placed in an agate mortar for full grinding, then transferred to a strip crucible, and placed in a high-temperature tubular furnace. It was pretreated at 350 °C for 3 h in Ar atmosphere, cooled and grinded again, and then sintered at 850 °C for 8 h in the tubular furnace to obtain the N-doped LVPC. According to the increasing order of doping nitrogen content, the synthesized products were recorded as LVPC/N-1, LVPC/N-2, LVPC/N-3, and LVPC/N-4, respectively. The specific synthetic routes are shown in Scheme 1. The synthesis process of LVPC is the same as that of N-doped LVPC, except that the reactant melamine was replaced with citric acid.

X-ray diffraction (XRD) measurements were carried on Rigaku MiniFlex 600 using Cu Kα radiation at $\lambda = 1.54$ Å. Scanning electron microscopy (SEM) and transmission electron microscope (TEM) were performed on FEI-Quanta 250 FEG and JEM-2100F, respectively. The obtained LVPC/N composite was mixed with super carbon black and poly tetra fluoroethylene (PTFE) microemulsion in a mass ratio of 8:1:1, and the mixture was dispersed in isopropanol, pressed into film, and dried at 80 °C for 10 h in a vacuum oven. Then the dried film was cut into a disk with a diameter of 10 mm and pasted on Al net. Electrochemical tests were carried using CR2016 coin-typed cells and the above electrode as cathode and Li metal as a counter electrode. Commercial polyethylene film and 1 mol L^{-1} $LiPF_6$ in ethylene carbonate and dimethyl carbonate (1:1 v/v) were employed as separator and electrolyte, respectively.

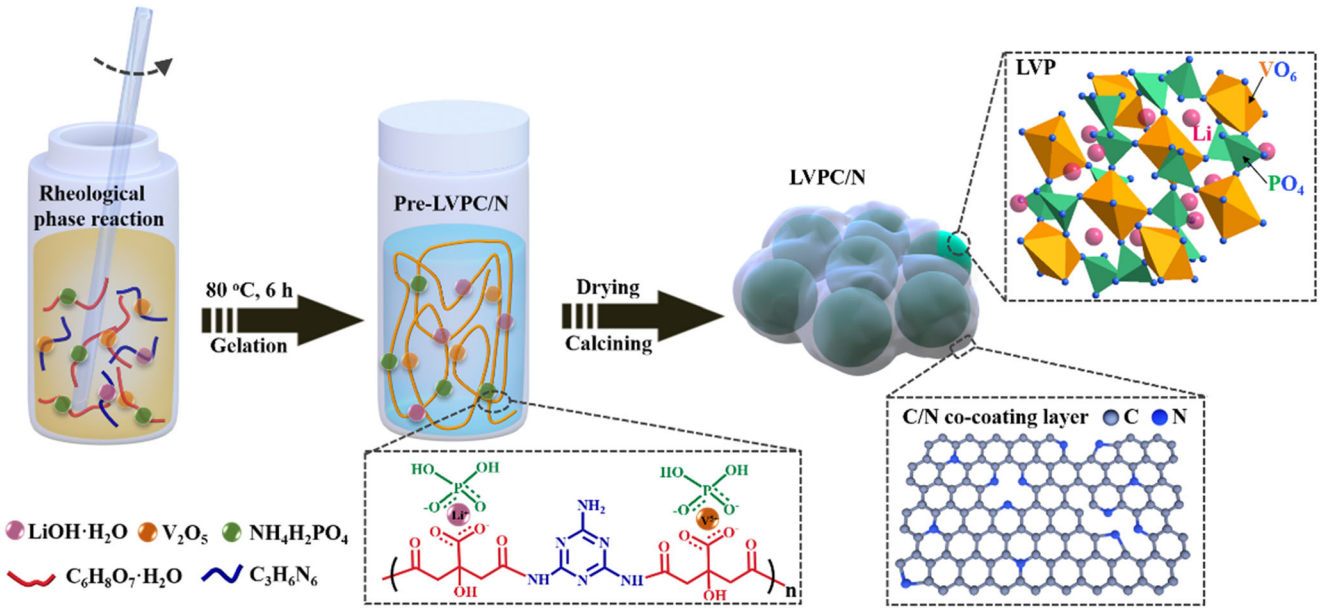

Scheme 1 Schematic illustration for formation process of LVPC/N

Galvanostatic charge/discharge tests were conducted on the CT 2001A battery tester (LAND) in the voltage range of 3.0–4.8 V (vs. Li^+/Li). Cyclic voltammetry (CV, 3.0–4.8 V (vs. Li^+/Li)) measurements and electrochemical impedance spectroscopy (EIS) (the frequency range is between 100 kHz and 10 mHz, potential amplitude: ± 5 mV) were tested on CHI 660E electrochemical workstation.

Results and discussion

Figure 1 shows the XRD spectra of pure carbon-coated LVP and carbon nitrogen co coated LVP materials. It can be seen from the figure that all LVPC/N samples have sharp diffraction peaks and no impurity peaks compared with LVPC sample. All of them belong to monoclinic LVP indexed to a space group of $P2_{1/n}$ (JCPDS No. 72-7074). Moreover, all samples have no other characteristic peaks, and the peaks of N-doped carbon are not found, indicating that the N-doped carbon is amorphous or mainly ascribed to its low content and the strong intensity of LVP peaks. It also states that N-doped carbon will not affect the crystal structure of the LVP. According to Raman spectra (Fig. 1b), the intensity ratio of D to G band (I_D/I_G) could estimate the defects in the graphitic carbon structure [40]. The I_D/I_G of LVPC/N-3 (0.96) is higher than that of LVPC (0.90), due to more defects structure caused by the incorporation of N atoms into carbon lattice.

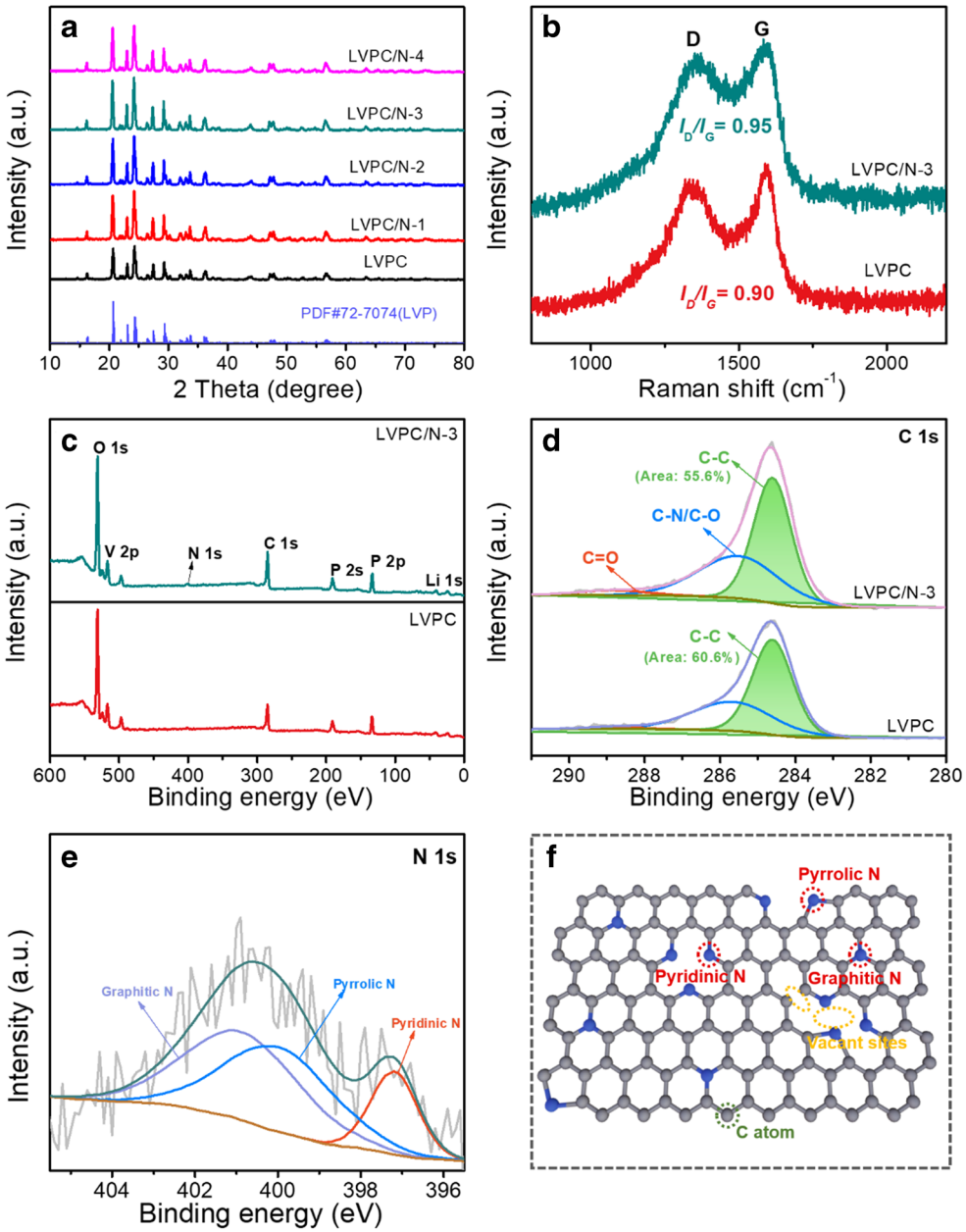

Fig. 1 (**a**) XRD patterns of LVPC and LVPC/N composites, (**b**) Raman spectra of LVPC and LVPC/N-3, (**c**) XPS surveys and (**d**) high resolution C 1s spectra of LVPC and LVPC/N-3, (**e**) XPS spectrum of N 1s for LVPC/N-3, and (**f**) the schematic illustration of N-doped carbon for LVPC/N composite

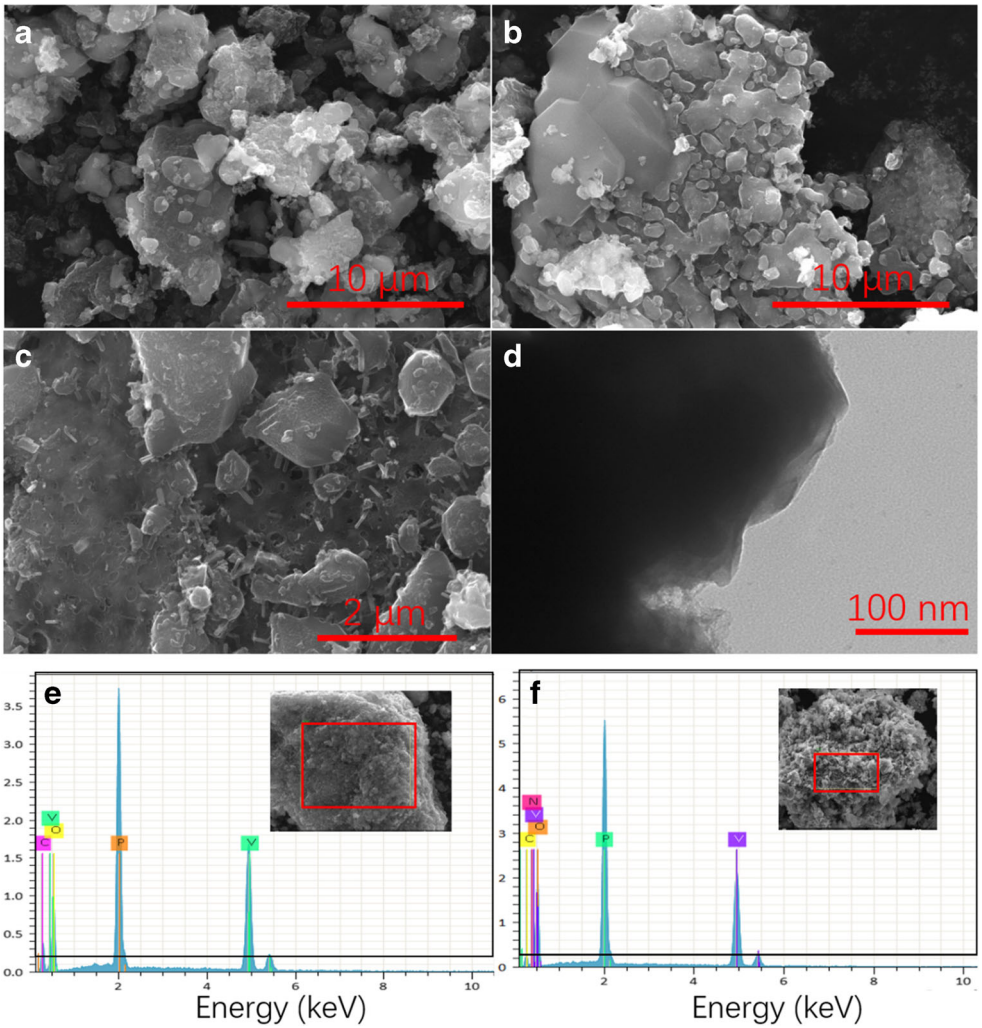

Fig. 2 SEM images of LVPC (**a**) and LVPC/N-3 composite (**b**, **c**), TEM image of LVPC/N-3 composite (**d**), energy-dispersive spectrometer (EDS) of LVPC (**e**), and LVPC/N-3 composite (**f**)

Moreover, XPS was performed to reveal the surface bonding information of the samples. In Fig. 1c, the signals of O, V, N, C, P, and Li elements are detected from the survey spectrum of LVPC/N, whereas there is no signal of N element in LVPC, which demonstrates that the N atoms have been successfully doped into LVPC/N composite and detected as 2.03 at.%. As displayed in Fig. 2d, the C 1s spectra of two samples can be resolved into three peaks located at 284.6, 285.6, and 288.8 eV, corresponding to the C–C, C–N/C–O, and C=O bond, respectively [41]. By comparison of the area percentage of C–C in total C, it is clearly seen that LVPC/N-3 shows a lower value of 55.6% than that of LVPC (60.6%), indicating more disorder carbon structure by N-doping. And in Fig. 1e, the characteristic N 1s spectrum of LVPC/N-3 can be divided into three N structures including pyridinic N (398.1 eV), pyrrolic N (399.6 eV), and graphitic N (401.2 eV) [42]. The schematic illustration of N-doped carbon structure was depicted as in Fig. 1f. With the well-designed structure, it could bring the mass vacant sites for Li-ion storage and boost the improvement of electron conductivity.

Table 1 The element content ratio of LVPC and LVPC/N-3 composite

Element	LVPCN-3		LVPC	
	Weight/ %	Atomic/ %	Weight/ %	Atomic/ %
O	41.49	55.21	30.05	38.28
C	9.92	17.58	22.02	37.36
P	21.42	14.72	20.13	13.24
V	26.14	10.93	27.80	11.12
N	1.03	1.57	0	0

The morphology of LVPC and LVPC/N-3 composite was investigated by SEM in Fig. 2a and b. As displayed in Fig. 2a, the LVPC consists of plate-like particles with about 2–5-μm diameters. Through Fig. 2b, it is easy to see that LVPC/N-3 composite shows a stacked bulk-like morphology with reduced sizes. Interestingly, there are uniform strip grains owing

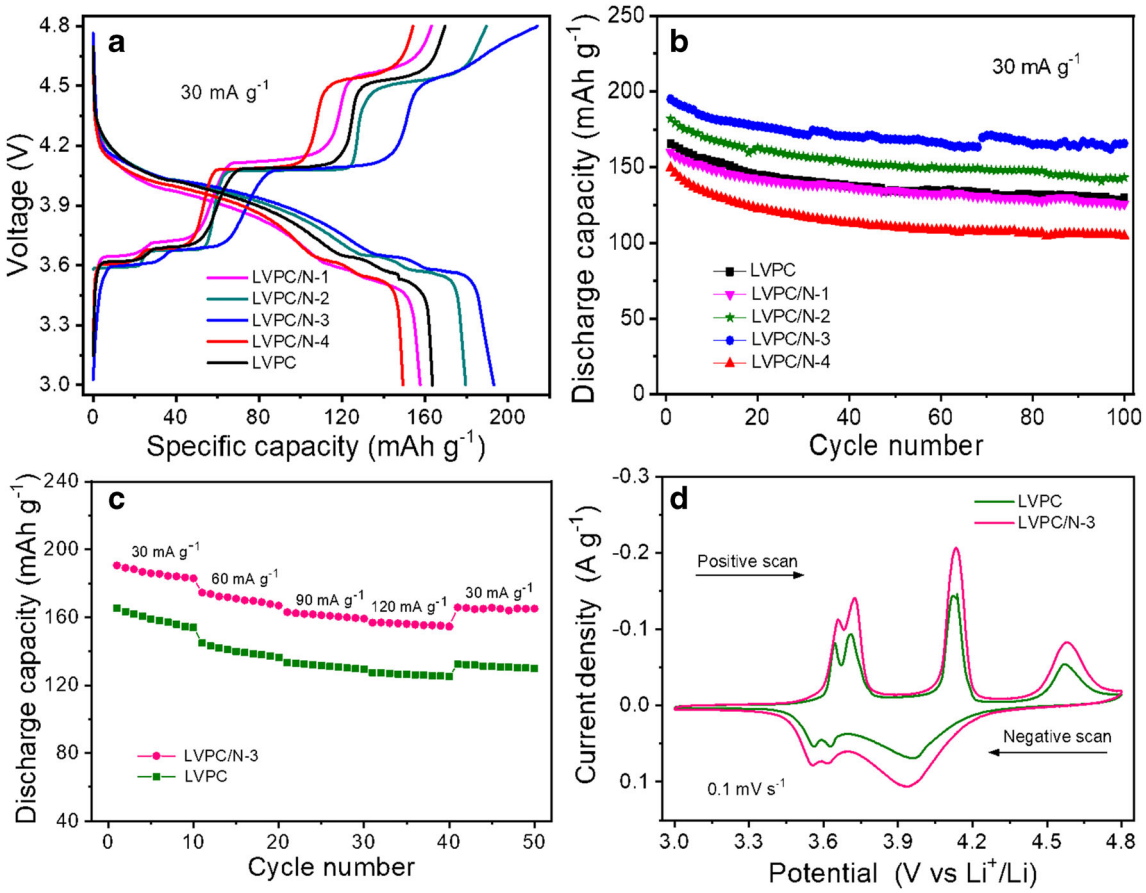

Fig. 3 Initial discharge curves (**a**) and cycle performances (**b**) of LVPC and four LVPC/N composites and rate capabilities (**c**) and CV curves (**d**) of LVPC and LVPC/N-3 composite

to the influences of N-doped carbon (Fig. 2c). It can be clearly seen from Fig. 2d that there is uniform N-doped carbon coating on the surface of LVP material, and the thickness is about 20 nm, which is in favor of the Li^+ ions insertion/extraction, bringing about the better electrochemical properties. EDS results in Fig. 2e described the existence of N compared to Fig. 2f, which more demonstrated that N-doped carbon is successfully composited with LVP. Table 1 illustrates the At % ratio of LVPC and LVPC/N-3 composite, further confirming the successful preparation of N-doped carbon-coated LVP.

Figure 3a shows the charge-discharge curves of LVPC and four LVPC/N composite electrodes in the second cycle at a voltage range of 3.0–4.8 V and a current density of 30 mA g^{-1}. As shown in the figure, the charge-discharge curves of all LVPC/N composites and LVPC are similar. The charging curves display four flat platforms, and the discharge curves display three platforms, which correspond to the phase change in the charge and discharge process, respectively, which are consistent with the literature reports [34, 43]. It shows that N-doped C does not affect the charge-discharge process behavior

Table 2 EIS equivalent circuit fitting parameters and the values of D_{Li}^+ for the LVPC and LVPC/N-3 composite at different cycle

Samples	Cycle	R_e (Ω)	R_f (Ω)	R_{ct} (Ω)	σ (Ω cm^2 s^{-1})	D_{Li}^+ (cm^2 s^{-1})
LVPC/N-3	1st	0.87	33.24	133.7	38.74	10.41×10^{-12}
	20th	1.735	51.09	59.09	23.26	28.88×10^{-12}
	50th	1.595	37.59	39.91	23.01	29.51×10^{-12}
	100th	1.971	28.43	36.24	16.24	59.25×10^{-12}
LVPC	1st	6.067	49.34	111.84	67.56	3.42×10^{-12}
	20th	0.608	4.13	16.10	26.75	21.84×10^{-12}
	50th	1.312	6.53	30.67	23.18	29.08×10^{-12}
	100th	1.541	7.56	42.62	24.01	27.10×10^{-12}

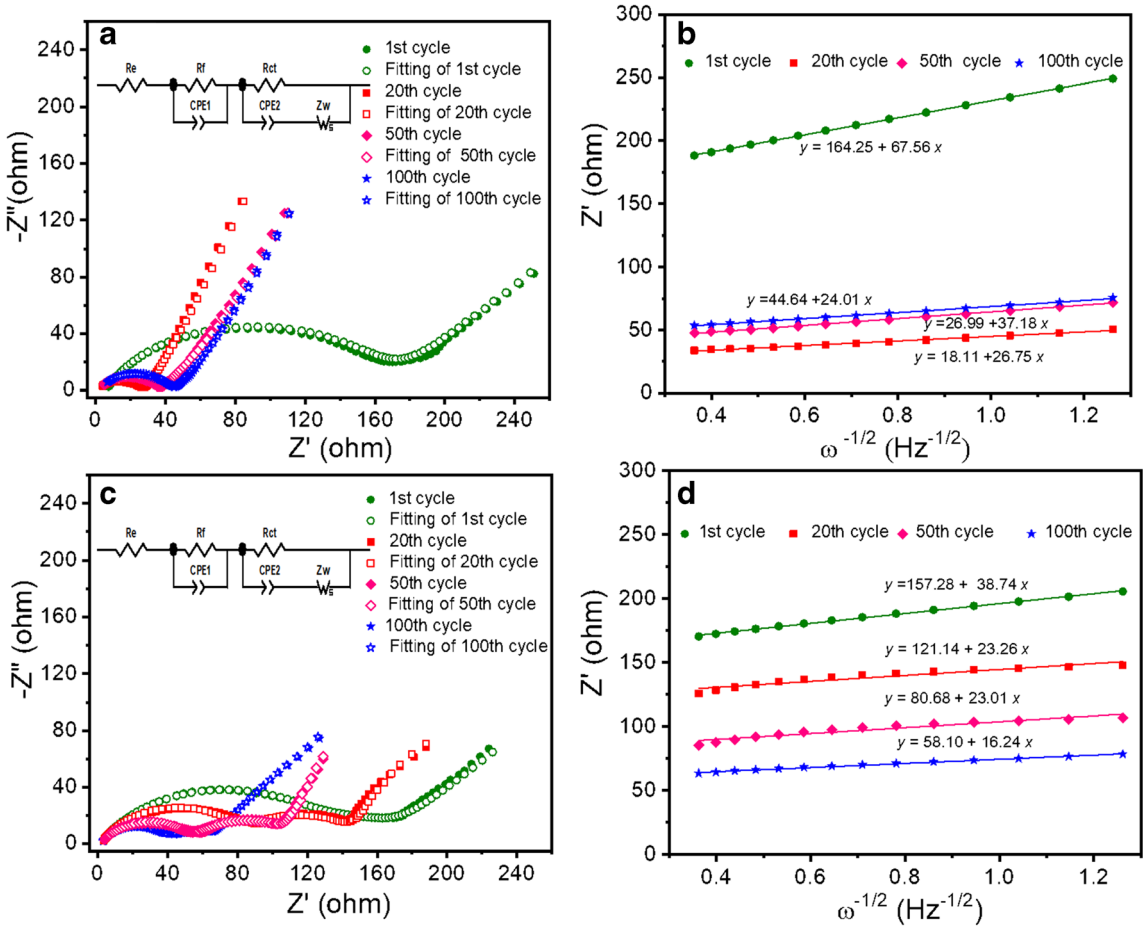

Fig. 4 The Nyquist plots of the LVPC (**a**) and LVPC/N-3 (**c**) and the relationship between Z′ and $\omega^{-1/2}$ of LVPC (**b**) and LVPC/N-3 (**d**) in the low-frequency region

of the LVPC. The discharge capacities of LVPC, LVPC/N-1, LVPC/N-2, LVPC/N-3, and LVPC/N-4 in the second cycle are 163.5, 157.6, 179.5, 193.1, and 146.3 mAh g^{-1}, respectively. Among them, LVPC/N-3 electrode has the highest discharge specific capacity, which is obviously improved compared with LVPC material, and the best ratio of citric acid to melamine is 1.25:0.75 (5:3). In addition, compared with LVPC, the charge-discharge voltage plateau of LVPC/N-2 and LVPC/N-3 is significantly longer, and the gap between charge and discharge platform is smaller, which indicates that the two electrode materials have higher capacity and better reversibility.

Figure 3b illustrates the cycle performance of LVPC and four LVPC/N composite electrodes in the same conditions. The initial discharge specific capacities of LVPC, LVPC/N-1, LVPC/N-2, LVPC/N-3, and LVPC/N-4 are 165.7, 160, 182.2, 195.0, and 149.7 mAh g^{-1}, respectively. After 100 cycles, the specific capacities and retention rates are 129.7 (78.3%), 125.5 (78.4%), 143.3 (78.6%), 165.7 (85.0%), and 104.7 mAh g^{-1} (70.0%), respectively. It is found that the discharge capacities and cycle performance of LVPC/N-1 and LVPC are almost the same; LVPC/N-2 and LVPC/N-3 materials have obvious improvement; especially LVPC/N-3 has the highest discharge capacity and the best cycle performance. However, the electrochemical performance of LVPC/N-4 material is poor, which may be due to the high proportion of melamine in the raw material, resulting in the thickness of the coating layer too low and the conductivity of the material poor. The results show that the amount of N-doped carbon should be suitable for the electrochemical performance of LVP.

In order to test the electrochemical performance of LVPC/N-3 material under different current density, the rate performance under continuous step current density compared with LVPC was carried out. The test results are shown in Fig. 3c. It can be seen from the figure that the discharge capacities of the materials are decreasing with the increase of current density, because the higher the current density is, the faster the charge-discharge is, and the greater the electrode polarization is. However, the discharge capacity of LVPC/N-3 is always higher than that of LVPC. And after 40 charging and discharging cycles at different current densities, the discharge capacity of LVPC/N-3 can still reach 165 mAh g^{-1} and the retention rate is 86%, while the capacity of LVPC material is only 132 mAh g^{-1} (80%), which indicates that N-doped carbon is more beneficial to the rate performance of LVP.

The CV curves of LVPC/N-3 and LVPC electrode materials at a scanning rate of 0.1 mV s^{-1} in the voltage range of 3.0–4.8 V are shown in Fig. 3d. From the figure, we can see that there are four oxidation peaks in the CV curves of the two materials, which are 3.64 V, 3.70 V, 4.13 V, and 4.56 V, respectively, which corresponds to the phase transition of $Li_3V_2(PO_4)_3 \longleftrightarrow Li_{2.5}V_2(PO_4)_3$, $Li_{2.5}V_2(PO_4)_3 \longleftrightarrow Li_2V_2(PO_4)_3$, $Li_2V_2(PO_4)_3 \longleftrightarrow Li_1V_2(PO_4)_3$, and $Li_1V_2(PO_4)_3 \longleftrightarrow V_2(PO_4)_3$. The three reduction peaks are 3.54 V, 3.64 V, and 4.01 V, respectively, and the reduction peak at 4.01 V represents the behavior of solid solution. The obvious difference is that the redox peak area of LVPC/N-3 is larger, which indicates that LVPC/N-3 has higher capacity. CV test results are consistent with constant current charge-discharge test results.

Figure 4 shows the EIS curves and equivalent circuit fitting diagram of LVPC and LVPC/N-3 electrodes after 1, 20, 50, and 100 charge and discharge cycles at 30 mA g^{-1} in the voltage range of 3.0–4.8 V. It can be seen from the figures that the Nyquist curve of LVPC is composed of a semicircle and a straight line, while the Nyquist curve of LVPC/N-3 consists of two flattened semicircles and a straight line, forming an obvious solid electrolyte interface (SEI). The fitting impedance value and calculated Li^+ ions diffusion coefficient (D_{Li}^+) results are shown in Table 2. The D_{Li}^+ can be calculated by the following equations: $Z' = R_e + R_f + R_{ct} + \sigma\omega^{-1/2}$ and $D_{Li^+} = 0.5\ R^2T^2/A^2n^4F^4C^2\sigma^2$ [44–46]. The comparison shows that the R_{ct} of the two materials is similar, which means that the charge transfer rate of lithium ions on the surface of the material and the internal diffusion rate of the material are the same. However, the R_f of LVPC/N-3 is significantly larger, and the D_{Li}^+ should also increase, which means that the Li^+ transfer process of LVPC/N-3 is changed during the charging and discharging process. The reason for this phenomenon is probably due to the N-doped carbon, which easily reacts with electrolyte to form SEI. SEI film is insoluble in organic solvents and can be stably stored in organic electrolyte. Lithium ions can pass through the passivation film freely, but solvent molecules cannot pass through it, which can effectively prevent the destruction of electrode materials caused by co-embedding of solvent molecules, thus greatly improving the cycle performance and service life of the electrode. Therefore, we speculate that N-doping does not change the intrinsic conductivity of LVPC but improves the lithium-ion migration rate and material stability by changing the coating layer; thus, improving the electrochemical performance of LVPC and LVPC/N-3 shows better rate performance and electrochemical cycle stability.

Conclusion

N-doped carbon-coated LVP composites were synthesized by one-step rheological phase method using melamine as nitrogen source and citric acid as carbon source. The effects of different ratios of melamine and citric acid on the structure and electrochemical properties of LVP were studied. The XRD results showed that the N-doped carbon did not affect the crystal structure of LVPC, and the electrochemical performance test results showed that when the ratio of citric acid to melamine was 5:3, the properties of LVPC/N-3 were the best. The initial discharge capacity of LVPC/N-3 is 195 mAh g^{-1} (LVPC, 165 mAh g^{-1}) at 30 mA g^{-1} in the voltage range of 3.0–4.8 V, and the capacity can still be maintained at 165 mAh g^{-1}(85%) (LVPC: 130 mAh g^{-1}, 78%) after 100 cycles. The effect of nitrogen doping on the LVPC was further explained from EIS. We found that the thickness and properties of the coating can be changed by adding melamine. On the one hand, N-doping can improve the conductivity of the coating. Even if the thickness of the coating is smaller, the conductivity of the material does not decrease. At the same time, the thinner N-doped carbon layer increases the tap density and the specific capacity of the material. On the other hand, N-doped carbon layer is conducive to the formation of SEI film, which can stabilize the electrode material and improve its cycle performance. Therefore, we conclude that this method can effectively improve the structure and electrochemical properties of LVP and can also be used for the modification of other electrode materials.

Funding This work was supported by the National Natural Science Foundation of China (Nos. 52071132, U1704142, and 21773057), Zhongyuan Thousand People Plan-The Zhongyuan Youth Talent Support Program (in Science and Technology), China (No. ZYQR201810139), and Fundamental Research Funds for the Henan Provincial Colleges and Universities in Henan University of Technology, China (No. 2018RCJH01).

References

1. Lin B, Zhu X, Fang L, Liu X, Li S, Zhai T, Xue L, Guo Q, Xu J, Xia H (2019) Birnessite nanosheet arrays with high K content as a high-capacity and ultrastable cathode for K-ion batteries. Adv Mater 31: 1900060
2. Zhu L, Li W, Xie L, Yang Q, Cao X (2019) Rod-like NaV_3O_8 as cathode materials with high capacity and stability for sodium storage. Chem Eng J 372:1056–1065
3. Kheimeh Sari HM, Li X (2019) Controllable cathode-electrolyte interface of $Li[Ni_{0.8}Co_{0.1}Mn_{0.1}]O_2$ for lithium ion batteries: a review. Adv Energy Mater 9:1901597
4. Zhu L, Ding G, Xie L, Cao X, Liu J, Lei X, Ma J (2019) Conjugated carbonyl compounds as high-performance cathode materials for rechargeable batteries. Chem Mater 31:8582–8612
5. Zhu L, Ge P, Xie L, Miao Y, Cao X (2020) Doped-$Li_{1+x}V_3O_8$ as cathode materials for lithium-ion batteries: a mini review. Electrochem Commun 115:106722
6. Yi T, Mei J, Peng P, Luo S (2019) Facile synthesis of polypyrrole-modified $Li_5Cr_7Ti_6O_{25}$ with improved rate performance as negative electrode material for Li-ion batteries. Compos Part B 167:566–572
7. Hou H, Banks CE, Jing M, Zhang Y, Ji X (2015) Carbon quantum dots and their derivative 3D porous carbon frameworks for sodium-ion batteries with ultralong cycle life. Adv Mater 27:7861–7866

8. Hong W, Zhang Y, Yang L, Tian Y, Ge P, Hu J, Wei W, Zou G, Hou H, Ji X (2019) Carbon quantum dot micelles tailored hollow carbon anode for fast potassium and sodium storage. Nano Energy 65:104038
9. Zhu L, Wang Z, Wang L, Xie L, Li J, Cao X (2019) ZnSe embedded in N-doped carbon nanocubes as anode materials for highperformance Li-ion batteries. Chem Eng J 364:503–513
10. Shi JL, Xiao DD, Ge M, Yu X, Chu Y, Huang X, Zhang XD, Yin YX, Yang XQ, Guo YG, Gu L, Wan LJ (2018) High-capacity cathode material with high voltage for Li-ion batteries. Adv Mater 30:1705575
11. Yang R, Zhang XJ, Fan TF, Jiang DP, Wang Q (2020) Improved electrochemical performance of ternary Sn-Sb-Cu nanospheres as anode materials for lithium-ion batteries. Rare Metals 39:1159–1164
12. Wang L, Wang Z, Xie L, Zhu L, Cao X (2019) ZIF-67-derived N-doped Co/C nanocubes as high-performance anode materials for lithium-ion batteries. ACS Appl Mater Interfaces 11:16619–16628
13. Zheng S, Li Q, Xue H, Pang H, Xu Q (2019) A highly alkaline-stable metal oxide@metal–organic framework composite for high-performance electrochemical energy storage. Natl Sci Rev 7:305–314
14. Wang L, Wang Z, Xie L, Zhu L, Cao X (2020) An enabling strategy for ultra-fast lithium storage derived from micro-flower-structured NiX (X=O, S, Se). Electrochim Acta 343:136138
15. Zheng S, Guo X, Xue H, Pan K, Liu C, Pang H (2019) Facile one-pot generation of metal oxide/hydroxide@metal–organic framework composites: highly efficient bifunctional electrocatalysts for overall water splitting. Chem Commun 55:10904–10907
16. Li X, Wei J, Li Q, Zheng S, Xu Y, Du P, Chen C, Zhao J, Xue H, Xu Q, Pang H (2018) Nitrogen-doped cobalt oxide nanostructures derived from cobalt–alanine complexes for high-performance oxygen evolution reactions. Adv Funct Mater 28:1800886
17. Zhu L, Bao C, Xie L, Yang X, Cao X (2020) Review of synthesis and structural optimization of $LiNi_{1/3}Co_{1/3}Mn_{1/3}O_2$ cathode materials for lithium-ion batteries applications. J Alloys Compd 831:154864
18. Jiao F, Shaju KM, Bruce PG (2005) Synthesis of nanowire and mesoporous low-temperature $LiCoO_2$ by a post-templating reaction. Angew Chem Int Edit 44:6550–6553
19. Fan L, Lei S, Kheimeh Sari HM, Zhong L, Kakimov A, Wang J, Chen J, Liu D, Huang L, Hu J, Lin L, Li X (2020) Controllable S-vacancies of monolayered Mo–S nanocrystals for highly harvesting lithium storage. Nano Energy 78:105235
20. Qian J, Zhou M, Cao Y, Ai X, Yang H (2010) Template-free hydrothermal synthesis of nanoembossed mesoporous $LiFePO_4$ microspheres for high-performance lithium-ion batteries. J Phys Chem C 114:3477–3482
21. Oh SW, Myung ST, Oh SM, Oh KH, Amine K, Scrosati B, Sun YK (2010) Double carbon coating of $LiFePO_4$ as high rate electrode for rechargeable lithium batteries. Adv Mater 22:4842–4845
22. Deng LZ, Wu F, Gao XG, Wu WP (2020) Development of a $LiFePO_4$-based high power lithium secondary battery for HEVs applications. Rare Metals 39:1457–1463
23. Tang M, Yuan A, Zhao H, Xu J (2013) High-performance $LiMn_2O_4$ with enwrapped segmented carbon nanotubes as cathode material for energy storage. J Power Sources 235:5–13
24. Lee HW, Muralidharan P, Ruffo R, Mari CM, Kim DK (2010) Ultrathin spinel $LiMn_2O_4$ nanowires as high power cathode materials for Li-ion batteries. Nano Lett 10:3852–3856
25. Li X, Yang X, Xue H, Pang H, Xu Q (2020) Metal–organic frameworks as a platform for clean energy applications. EnergyChem 2:100027
26. Cao X, Mo L, Zhu L, Xie L (2017) Preparation and electrochemical properties of $Li_3V_2(PO_4)_{3-x}Br_x$/carbon composites as cathode materials for lithium-ion batteries. Nanomaterials 7:52
27. Ren MM, Zhou Z, Gao XP, Peng WX, Wei JP (2008) Core−shell $Li_3V_2(PO_4)_3$@C composites as cathode materials for lithium-ion batteries. J Phys Chem C 112:5689–5693
28. Li Y, Zhou Z, Ren M, Gao X, Yan J (2006) Electrochemical performance of nanocrystalline $Li_3V_2(PO_4)_3$/carbon composite material synthesized by a novel sol-gel method. Electrochim Acta 51:6498–6502
29. Zhu L, Yang J, Cao X (2015) Graphene modified $Li_3V_2(PO_4)_3$/C composites with improved electrochemical performances as cathode materials for Li-ion batteries. Int J Electrochem Sci 10:6509–6516
30. Liu H, Gao P, Fang J, Yang G (2011) $Li_3V_2(PO_4)_3$/graphene nanocomposites as cathode material for lithium ion batteries. Chem Commun 47:9110–9112
31. Cao X, Wu H, Ge P, Zhao Y, Zhu L, Liu F, Wang J (2015) Synthesis of $Li_3V_2(PO_4)_3$/C composites as cathode materials for lithium ion batteries via a sol-gel method. Int J Electrochem Sc 10:2997–3009
32. Zhu LM, Sun QH, Xie LL, Cao XY (2020) $Na_3V_2(PO_4)_3$@NC composite derived from polyaniline as cathode material for high-rate and ultralong-life sodium-ion batteries. Int J Energy Res 44:4586–4594
33. Ge P, Hou H, Li S, Yang L, Ji X (2018) Tailoring rod-like $FeSe_2$ coated with nitrogen-doped carbon for high-performance sodium storage. Adv Funct Mater 28:1801765
34. Cui K, Hu SC, Li YK (2016) Nitrogen-doped graphene nanosheets decorated $Li_3V_2(PO_4)_3$/C nanocrystals as high-rate and ultralong cycle-life cathode for lithium-ion batteries. Electrochim Acta 210:45–52
35. Wang F, Wang Y, Xu J, Huang K (2020) A high-energy sandwich-type self-powered biosensor based on DNA bioconjugates and a nitrogen doped ultra-thin carbon shell. J Mater Chem B 8:1389–1395
36. Xing L, Huang K, Cao S, Pang H (2018) Chestnut shell-like $Li_4Ti_5O_{12}$ hollow spheres for high-performance aqueous asymmetric supercapacitors. Chem Eng J 332:253–259
37. Darwiche A, Bodenes L, Madec LC, Monconduit L, Martinez H (2016) Impact of the salts and solvents on the SEI formation in Sb/Na batteries: an XPS analysis. Electrochim Acta 207:284–292
38. Xie X, Huang K, Wu X, Wu N, Xu Y, Zhang S, Zhang C (2020) Binding hierarchical $MoSe_2$ on MOF-derived N-doped carbon dodecahedron for fast and durable sodium-ion storage. Carbon 169:1–8
39. Zhai Z, Huang K, Wu X, Hu H, Xu Y, Chai R (2019) Metal–organic framework derived small sized metal sulfide nanoparticles anchored on N-doped carbon plates for high-capacity energy storage. Dalton Trans 48:4712–4718
40. Zhu T, Liu S, Wan K, Zhang C, Feng Y, Feng W, Liu T (2020) Fluorine and nitrogen dual-doped porous carbon nanosheet-enabled compact electrode structure for high volumetric energy storage. ACS Appl Energy Mater 3:4949–4957
41. Chen Y, Xiang K, Zhu Y, Xiao L, Chen W, Chen X, Chen H (2019) Bio-template fabrication of nitrogen-doped $Li_3V_2(PO_4)_3$/carbon composites from cattail fibers and their high-rate performance in lithium-ion batteries. J Alloys Compd 782:89–99
42. Mu T, Zuo P, Lou S, Pan Q, Li Q, Du C, Gao Y, Cheng X, Ma Y, Yin G (2018) A two-dimensional nitrogen-rich carbon/silicon composite as high performance anode material for lithium ion batteries. Chem Eng J 341:37–46
43. Rui XH, Yan QY, Skyllas-Kazacos M, Lim TM (2014) $Li_3V_2(PO_4)_3$ cathode materials for lithium-ion batteries: a review. J Power Sources 258:19–38
44. Zhu L, Xie L, Cao X (2018) LiV_3O_8/polydiphenylamine composites with significantly improved electrochemical behavior as cathode materials for rechargeable lithium batteries. ACS Appl Mater Interfaces 10:10909–10917

45. Ding GC, Zhu LM, Yang Q, Xie LL, Cao XY, Wang YL, Liu JP, Yang XL (2020) NaV_3O_8/poly(3,4-ethylenedioxythiophene) composites as high-rate and long-lifespan cathode materials for reversible sodium storage. Rare Metals 39:865–873
46. Xu Q, Li X, Kheimeh Sari HM, Li W, Liu W, Hao Y, Qin J, Cao B, Xiao W, Xu Y, Wei Y, Kou L, Tian Z, Shao L, Zhang C, Sun X (2020) Surface engineering of $LiNi_{0.8}Mn_{0.1}Co_{0.1}O_2$ towards boosting lithium storage: bimetallic oxides versus monometallic oxides. Nano. Energy 77:105034